

# A Low-Cost Attitude Determination System using Multiple Sensors for High-Altitude Balloon Flights

Ankit Jain\* and Douglas R. Isenberg<sup>†</sup>

*Embry-Riddle Aeronautical University, Prescott, AZ, 86301, USA*

This paper discusses the calibration and implementation of a low-cost attitude determination system for high-altitude balloon flights using multiple sensors. The attitude determination system is comprised of a 3-axis accelerometer and a sun sensor. The accelerometer is utilized to measure the gravitational acceleration vector of the payload in the payload's body frame. The measured acceleration vector is based upon the accelerometer's bias and sensitivity which can be found through calibration under zero motion conditions. The sun sensor is comprised of many solar cells at various angles. These are utilized to obtain an accurate sunlight directional vector of the payload in the payload's body frame from an over-determined system of measurement equations. The development of these equations is discussed. Both the gravitational acceleration vector and the sunlight directional vector can also be measured in an inertial frame. It is assumed that these measurements are known a-priori. This provides enough information to solve for an attitude at each sample instance, utilizing two independent vector measurements (i.e., the sunlight and acceleration vectors). The attitude determination system utilizes Markley's solution to Wahba's problem. A 3-axis rate gyroscope is also utilized to gather angular velocity information of the payload in the payload's body frame and was used to compare against angular velocity derived from the estimated attitude to validate the accuracy of the attitude determination system. The measured angular velocity vector is based upon the rate gyroscope's bias and sensitivity which can be found through calibration under zero motion conditions.

## I. Introduction

The attitude of a body is the orientation of the body, which can be expressed in various frames of reference. Nowadays, attitude control mechanisms are being implemented in many dynamic systems such as satellites, aircrafts, robotics, etc. To control the attitude of an object successfully, one must determine the attitude of the object accurately. There are many systems available in the market that use expensive sensors and hardware to take care of attitude determination for safety critical systems. The problem is creating an accurate, low-cost attitude determination system that can be implemented in a real-time system, for low-cost applications such as high-altitude balloon payloads.

There is a growing interest in high-altitude balloon payloads for scientific and educational purposes. It is very expensive to put a satellite in space using a launch vehicle. Thus, high-altitude balloon payloads are an economical alternative to using launch vehicles for scientific experiments to be conducted at high altitudes (i.e., roughly 60,000 to 120,000 ft.). These types of scientific experiments are typically Earth-related observations including geological and atmospheric observations.

Project Loon is a developing project, by Google, with an objective to provide internet to rural and remote areas using high-altitude balloon payloads.<sup>1</sup> They will be using a heading/position control system as the payloads need to be pointing in the proper orientation (i.e., attitude) to successfully provide internet to certain areas. Project Loon is just one example of the possible future developments and applications from high-altitude ballooning. Previous work has been done regarding attitude determination and control for high-altitude balloon systems. Examples of such work include publications on an attitude system for

---

\*Student, Department of Aerospace and Mechanical Engineering, 3700 Willow Creek Rd., Prescott, AZ 86301, AIAA Student Member.

<sup>†</sup>Assistant Professor, Department of Aerospace and Mechanical Engineering, 3700 Willow Creek Rd., Prescott, AZ 86301.

ultrahigh altitude flights<sup>2</sup> ; Earth-related observations from a high-altitude balloon system<sup>3</sup> ; and testing for acquisition, tracking, and pointing technologies from a high-altitude balloon experiment.<sup>4</sup>

This paper discusses an attitude determination system that can be implemented using low-cost sensors for high-altitude balloon payloads. The sensors exploited in this paper include a sun sensor made of solar cells, and an Inertial Measurement Unit (IMU) consisting of a 3-axis accelerometer and a 3-axis rate gyroscope. The calibration and implementation process for each of the sensors is also discussed in the paper. The attitude determination algorithm uses the Singular Value Decomposition (SVD) method to solve for an attitude from the measured and observer based vectors. By analyzing the data from a flight and comparing the angular velocity information gathered from the rate gyroscope against the angular velocity information computed from the estimated attitude, the accuracy of the attitude determination system will be determined along with the validity of the proposed system.

## II. Attitude Determination

There are many parameterizations that are available to quantify attitude. Some of the most commonly used include Euler Angles, Direction Cosine Matrix (DCM), Quaternions, and Euler Parameters. DCMs are used in this paper to parameterize the attitude of a body. If there exists two vectors in two unique reference frames  $A$  and  $B$ , one can rotate the vector measurements of frame  $B$  into frame  $A$  using the relationship described by:

$$\mathbf{r}^A = T_B^A \mathbf{r}^B \quad (1)$$

where  $\mathbf{r}^A$  and  $\mathbf{r}^B$  are the two vectors in frames  $A$  and  $B$ , respectively, and  $T_B^A$  is the DCM whose columns describe the unit basis vectors of  $B$  in  $A$ .

In the past, there have been quite a few attitude estimation algorithms that have been proposed and experimentally validated for certain applications. Examples include an extended Kalman-based linear fusion algorithm<sup>5</sup> ; attitude determination systems using various methods of Kalman filtering<sup>6</sup> ; a gyro-free Quaternion-based attitude determination system with Kalman filtering<sup>7</sup> ; an attitude heading reference system by combination of GPS, magnetometers, and MEMS inertial sensors<sup>8</sup> ; and others.

The attitude determination or estimation algorithm proposed here is a combination of Wahba's problem<sup>9</sup> and Markley's SVD solution to Wahba's problem<sup>10</sup> . Wahba's problem is depicted below where the purpose of the problem is to minimize the cost function:

$$\min_{T_B^A} J = \frac{1}{2} \sum_{n=1}^N a_n \|\mathbf{r}_n^A - T_B^A \mathbf{r}_n^B\|^2 \quad (2)$$

where  $J$  is the cost function that is to be minimized.  $N$  is the number of independent unit-vectors and  $N \geq 2$  for a unique solution. These independent unit-vectors could be the acceleration vector, magnetic field vector, sunlight vector, etc.  $a_n$  are the weights for the various independent unit-vectors and are used to filter noisy measurements; i.e. a noisy vector measurement is weighted less compared to that of a reliable vector measurement, which is weighted more.  $\mathbf{r}_n^A$  and  $\mathbf{r}_n^B$  are the unit-vector measurements in frames  $A$  and  $B$ , the inertial frame and body frame, respectively.  $T_B^A$  is the orthonormal matrix that is described by the relationship in (1), and has a determinant of +1.

The attitude determination system proposed here uses two independent unit-vector measurements. Thus,  $N = 2$ . These unit-vectors are the unit-sunlight vector and the unit-acceleration vector. Since  $N = 2$ , an attitude can be found as a unique solution to Wahba's problem exists.

There are various methods that can be utilized to solve Wahba's Problem such as Davenport's q-Method<sup>11</sup> , the QUEST algorithm<sup>12</sup> , and Markley's SVD solution<sup>13</sup> . The proposed attitude determination system uses Markley's SVD solution<sup>10</sup> . For the implementation of the SVD method, (2) must be rewritten:

$$\begin{aligned} \min_{T_B^A} J &= \frac{1}{2} \sum_{n=1}^N a_n (\|\mathbf{r}_n^A\|^2 - \|\mathbf{r}_n^B\|^2) - \sum_{n=1}^N a_n (\mathbf{r}_n^A)^T T_B^A \mathbf{r}_n^B \\ &= \sum_{n=1}^N a_n - \text{trace}\{T_B^A B^T\} \end{aligned} \quad (3)$$

where

$$B = \sum_{n=1}^N a_n \mathbf{r}_n^A (\mathbf{r}_n^B)^T \quad (4)$$

Thus,  $B$  must be created based on the relationship described above.  $B$  will be a  $3 \times 3$  matrix as both  $\mathbf{r}_n^A$  and  $\mathbf{r}_n^B$  are  $3 \times 1$  column vectors. For  $N = 2$ , (4) can be written as the following:

$$B = (a_S \mathbf{r}_S^A (\mathbf{r}_S^B)^T) + (a_A \mathbf{r}_a^A (\mathbf{r}_a^B)^T) \quad (5)$$

where the subscript  $S$  corresponds to the sunlight vector and subscript  $a$  corresponds to the acceleration vector.  $\mathbf{r}_S^B$  and  $\mathbf{r}_a^B$  are the body frame unit-vector measurements. Thus, they are measured from the sensor data and are discussed later.  $\mathbf{r}_S^A$  and  $\mathbf{r}_a^A$  are the inertial frame vectors which must be defined for a specific reference frame.

The acceleration vector in the inertial frame is the acceleration due to the gravitational field of the Earth and is assumed to have a constant component only along the z-axis of the inertial frame. For the current research, the attitude estimate is verified indirectly through the use of body measured angular velocity which is invariant to a specific choice of inertial frame. Thus, the orientation of the x-axis and y-axis of the inertial frame are defined based upon the initial sunlight vector. The initial sunlight vector in the inertial frame is obtained from the sun sensor during the initial instance of the flight at a point in time when the measured gravity vector has components only along the z-axis. Therefore,  $\mathbf{r}_S^A$  and  $\mathbf{r}_a^A$  are defined as the following:

$$\mathbf{r}_S^A = \begin{bmatrix} 0.4449 \\ -0.7122 \\ -0.5430 \end{bmatrix}, \quad \mathbf{r}_a^A = \begin{bmatrix} 0 \\ 0 \\ 1 \end{bmatrix} \quad (6)$$

Note that both  $\mathbf{r}_S^A$  and  $\mathbf{r}_a^A$  are normalized so they have unit magnitude. It is also very important that  $\mathbf{r}_S^B$  and  $\mathbf{r}_a^B$  are normalized as well before being implemented into (4). The  $\mathbf{r}_S^A$  vector can also be defined using azimuth and elevation data from databases, such as the NOAA<sup>14</sup> database, based on latitude and longitude data, to account for the rotation of the Earth. The azimuth and elevation data would have to be transformed into the inertial frame.

Once matrix  $B$  is properly defined, the SVD of matrix  $B$  is found as:

$$U \Sigma V^T = B \quad (7)$$

where  $U$  and  $V$  are orthogonal matrices and  $\Sigma$  is a diagonal matrix of the singular values of  $B$ . The SVD of matrix  $B$  can be computed quite easily using MATLAB's built-in SVD function call. After the SVD of matrix  $B$  is determined, one can form an estimate of  $T_B^A$  as the following:

$$T_B^A = U \begin{bmatrix} 1 & 0 & 0 \\ 0 & 1 & 0 \\ 0 & 0 & |U||V| \end{bmatrix} V^T \quad (8)$$

Since the measured body frame vectors have unique values for different instances (i.e., samples), the resulting  $T_B^A$  would have to be computed at each of the sampling instances, thus solving for an attitude of the body with respect to the inertial frame for each sampling instance.

To obtain the sunlight vector and the acceleration vector in the body frame, low-cost sensors were implemented. The sunlight vector in the body frame was obtained using a sun sensor comprised of solar cells which measured light intensity information. The acceleration vector of the body frame was obtained using an accelerometer. The following describes how to obtain the above mentioned body frame vectors from the low-cost sensors that were implemented.

## A. Sunlight Vector from Solar Cells

The sunlight vector measurements in the body frame can be measured using solar cells or photovoltaic cells. There are a few assumptions involved in using solar cells as a sun sensor. One of these assumptions includes the fact that the solar cell is a flat device and can only measure light readings from one side.

Another assumption involved in using solar cells as a sun sensor is that the solar cell can only pick up normal components of light. Therefore, it is assumed that the parallel component of the incoming light is not detectable by the solar cells due to the non-refractive properties of the solar cell. This is depicted in Fig. 1.

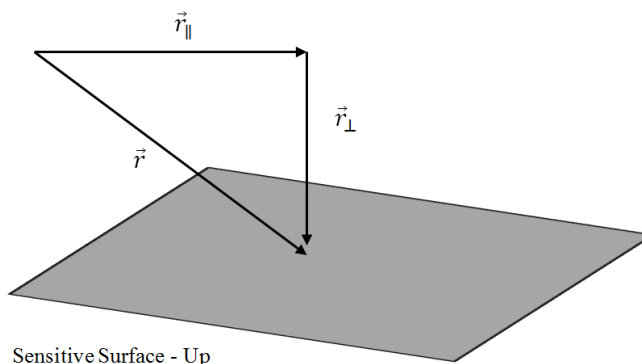


**Figure 1.** Sensitive surface of the solar cell.

As depicted by Fig. 1, the solar cell has only one sensitive surface that can detect the perpendicular component of the incoming light vector. Another assumption involved with using solar cells as a sun sensor is that each solar cell can only measure the positive-component information. For example, two solar cells would be required to describe the (+) x-component and (-) x-component of light information for a body.

For a given structure geometry and the respective angles between each surface, one can form a system of mathematical equations that describes the transformation from each surface frame (i.e., solar cell frame) to a given body frame. These transformations can be performed using the transformation matrices described below:

$$Rot_X(\theta) = \begin{bmatrix} 1 & 0 & 0 \\ 0 & \cos\theta & -\sin\theta \\ 0 & \sin\theta & \cos\theta \end{bmatrix} \quad (9)$$

$$Rot_Y(\theta) = \begin{bmatrix} \cos\theta & 0 & \sin\theta \\ 0 & 1 & 0 \\ -\sin\theta & 0 & \cos\theta \end{bmatrix} \quad (10)$$

$$Rot_Z(\theta) = \begin{bmatrix} \cos\theta & -\sin\theta & 0 \\ \sin\theta & \cos\theta & 0 \\ 0 & 0 & 1 \end{bmatrix} \quad (11)$$

where  $Rot_X(\theta)$ ,  $Rot_Y(\theta)$ , and  $Rot_Z(\theta)$  are the transformation matrices that rotates a given frame about the x-axis, y-axis, and z-axis; respectively.  $\theta$  is the angle by which one would like to rotate about, for the respective rotation axis. Also, note that it only takes two rotations to go from one frame to another.

Since the solar cell only gathers light information that is perpendicular to its own surface, one can make each surface frame (i.e., each solar cell frame) align with a certain axis component that is always normal to the surface. For example, the (+) x-axis of each surface frame is always perpendicular to and points out of the respective surface. After one obtains the body frame vector measurements, they can be normalized to form the  $\mathbf{r}_S^B$  vector to be used in SVD solution method that was described earlier.

For the flight from which the data in this paper is presented, a payload consisting of 26 sides was used. The structure was made to have 26 surfaces due to the relative  $45^\circ$  angle between each surface, and to increase the accuracy of the light vector measurement information in the body frame. Fig. 2 depicts how the solar cells were oriented to construct the sun sensor.



Figure 2. Sun sensor implementation on payload.

As depicted by Fig. 2, each solar cell is mounted on a surface that is angled  $45^\circ$  from its adjacent surfaces. Due to physical limitations, there was no solar cell placed on the top and bottom surfaces of the payload. There was also a surface with a camera window. Therefore, out of the 26 surfaces of the payload, 23 of them were affixed with solar cells in order to construct the sun sensor array. The solar cells that were used to implement the sun sensor are SP3-37 solar cells from PowerFilm Solar Inc. The outputs of each of these solar cells is amplified using TLV2454 rail-to-rail linear operational amplifiers (OPAMPs) in non-inverting configurations as depicted in Fig. 3.

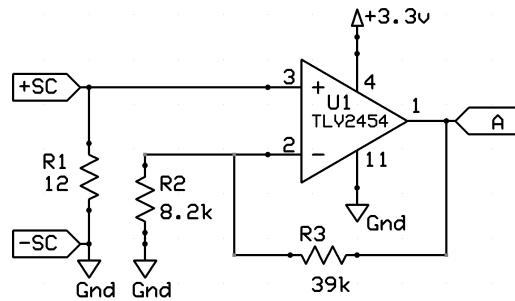


Figure 3. Solar cell signal conditioning circuit.

Once the solar cell output signals are conditioned using the OPAMPs, the amplified signals can be used to form the body frame vector of the sunlight information. To form the body frame light vector measurements from the 23 solar cells, for the payload described above, the set of rotations can be categorized into the three regions of the payload: the middle layer, the top layer, and the bottom layer.

A body frame reference needs to be defined before each of the regions of the payload is analyzed for their respective transformations. The body frame was defined with the (+) x-axis being perpendicular to and pointing out of the surface with the solar cell SC1, the (+) y-axis being perpendicular to and pointing out of the surface with the solar cell SC3, and the (+) z-axis being perpendicular to and pointing out of the top surface of the payload. Fig. 4 depicts the body frame setup in the Cartesian coordinate system.

In Fig.4, the top layer (i.e., SC9 to SC16) is identified by the underlined solar cells, the middle layer (i.e., SC1 to SC8) is identified by the bolded solar cells, and the bottom layer (i.e., SC17 to SC23) is identified by the italicized solar cells. Note that one of the bottom layer solar cells is missing, between SC21 and SC22, which is the camera window (as mentioned earlier). A surface frame is assigned to each solar cell surface such that the (+) x-axis is normal to and points out of the sensor surface. Since a solar cell can only measure the normal component of the incoming light vector, each reading is going to be only along the x-axis of the assigned surface frames. Using the transformation matrices defined in (9), (10), and (11), mathematical

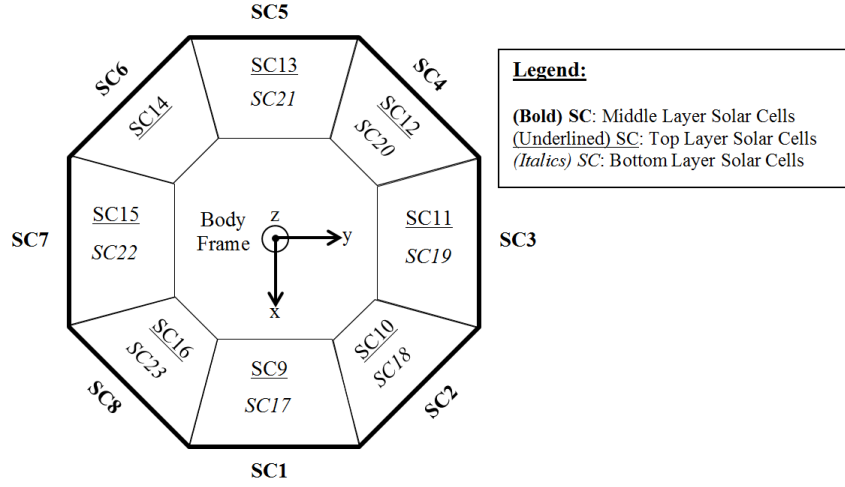


Figure 4. Sensor frame references for solar cells.

relationships can be formed for each solar cell that describe the solar cell measurement,  $A_i$ , in terms of the components of  $\mathbf{r}_S^B$ . The middle layer solar cell relationships can be depicted from the following:

$$\begin{aligned}
 A_1 &= [1 \ 0 \ 0] (I)^T \mathbf{r}_S^B \\
 A_2 &= [1 \ 0 \ 0] (\text{Rot}_Z(\pi/4))^T \mathbf{r}_S^B \\
 A_3 &= [1 \ 0 \ 0] (\text{Rot}_Z(\pi/2))^T \mathbf{r}_S^B \\
 A_4 &= [1 \ 0 \ 0] (\text{Rot}_Z(3\pi/4))^T \mathbf{r}_S^B \\
 A_5 &= [1 \ 0 \ 0] (\text{Rot}_Z(\pi))^T \mathbf{r}_S^B \\
 A_6 &= [1 \ 0 \ 0] (\text{Rot}_Z(5\pi/4))^T \mathbf{r}_S^B \\
 A_7 &= [1 \ 0 \ 0] (\text{Rot}_Z(3\pi/2))^T \mathbf{r}_S^B \\
 A_8 &= [1 \ 0 \ 0] (\text{Rot}_Z(7\pi/4))^T \mathbf{r}_S^B
 \end{aligned} \tag{12}$$

Similarly, the top layer solar cell relationships can be depicted from the following:

$$\begin{aligned}
 A_9 &= [1 \ 0 \ 0] (\text{Rot}_Y(-\pi/4))^T \mathbf{r}_S^B \\
 A_{10} &= [1 \ 0 \ 0] (\text{Rot}_Z(\pi/4) \text{Rot}_Y(-\pi/4))^T \mathbf{r}_S^B \\
 A_{11} &= [1 \ 0 \ 0] (\text{Rot}_Z(\pi/2) \text{Rot}_Y(-\pi/4))^T \mathbf{r}_S^B \\
 A_{12} &= [1 \ 0 \ 0] (\text{Rot}_Z(3\pi/4) \text{Rot}_Y(-\pi/4))^T \mathbf{r}_S^B \\
 A_{13} &= [1 \ 0 \ 0] (\text{Rot}_Z(\pi) \text{Rot}_Y(-\pi/4))^T \mathbf{r}_S^B \\
 A_{14} &= [1 \ 0 \ 0] (\text{Rot}_Z(5\pi/4) \text{Rot}_Y(-\pi/4))^T \mathbf{r}_S^B \\
 A_{15} &= [1 \ 0 \ 0] (\text{Rot}_Z(3\pi/2) \text{Rot}_Y(-\pi/4))^T \mathbf{r}_S^B \\
 A_{16} &= [1 \ 0 \ 0] (\text{Rot}_Z(7\pi/4) \text{Rot}_Y(-\pi/4))^T \mathbf{r}_S^B
 \end{aligned} \tag{13}$$

Lastly, the bottom layer solar cell relationships can be depicted from the following:

$$\begin{aligned}
A_{17} &= [ 1 \ 0 \ 0 ] (Rot_Y(\pi/4))^T \mathbf{r}_S^B \\
A_{18} &= [ 1 \ 0 \ 0 ] (Rot_Z(\pi/4)Rot_Y(\pi/4))^T \mathbf{r}_S^B \\
A_{19} &= [ 1 \ 0 \ 0 ] (Rot_Z(\pi/2)Rot_Y(\pi/4))^T \mathbf{r}_S^B \\
A_{20} &= [ 1 \ 0 \ 0 ] (Rot_Z(3\pi/4)Rot_Y(\pi/4))^T \mathbf{r}_S^B \\
A_{21} &= [ 1 \ 0 \ 0 ] (Rot_Z(\pi)Rot_Y(\pi/4))^T \mathbf{r}_S^B \\
A_{22} &= [ 1 \ 0 \ 0 ] (Rot_Z(3\pi/2)Rot_Y(\pi/4))^T \mathbf{r}_S^B \\
A_{23} &= [ 1 \ 0 \ 0 ] (Rot_Z(7\pi/4)Rot_Y(\pi/4))^T \mathbf{r}_S^B
\end{aligned} \tag{14}$$

Panels SC9, SC10, SC11, SC12, and SC13 did not perform as expected due to faulty wiring, so they have been removed from further discussion. The above described middle, top, and bottom layer equations are combined together to form a system of equations:

$$\begin{bmatrix} A_1 \\ A_2 \\ A_3 \\ A_4 \\ A_5 \\ A_6 \\ A_7 \\ A_8 \\ A_{14} \\ A_{15} \\ A_{16} \\ A_{17} \\ A_{18} \\ A_{19} \\ A_{20} \\ A_{21} \\ A_{22} \\ A_{23} \end{bmatrix} = \begin{bmatrix} 1 & 0 & 0 \\ \frac{\sqrt{2}}{2} & \frac{\sqrt{2}}{2} & 0 \\ 0 & 1 & 0 \\ -\frac{\sqrt{2}}{2} & \frac{\sqrt{2}}{2} & 0 \\ -1 & 0 & 0 \\ -\frac{\sqrt{2}}{2} & -\frac{\sqrt{2}}{2} & 0 \\ 0 & -1 & 0 \\ \frac{\sqrt{2}}{2} & -\frac{\sqrt{2}}{2} & 0 \\ -\frac{1}{2} & -\frac{1}{2} & \frac{\sqrt{2}}{2} \\ 0 & -\frac{\sqrt{2}}{2} & \frac{\sqrt{2}}{2} \\ \frac{1}{2} & -\frac{1}{2} & \frac{\sqrt{2}}{2} \\ \frac{\sqrt{2}}{2} & 0 & -\frac{\sqrt{2}}{2} \\ \frac{1}{2} & \frac{1}{2} & -\frac{\sqrt{2}}{2} \\ 0 & \frac{\sqrt{2}}{2} & -\frac{\sqrt{2}}{2} \\ -\frac{1}{2} & \frac{1}{2} & -\frac{\sqrt{2}}{2} \\ -\frac{\sqrt{2}}{2} & 0 & -\frac{\sqrt{2}}{2} \\ 0 & -\frac{\sqrt{2}}{2} & -\frac{\sqrt{2}}{2} \\ \frac{1}{2} & -\frac{1}{2} & -\frac{\sqrt{2}}{2} \end{bmatrix} \mathbf{r}_S^B \tag{15}$$

Here, none of the  $A_i$  terms can have a value of 0. Thus, an algorithm has to be implemented such that if one of the  $A_i$  terms does have a value of 0, then the corresponding equation for  $A_i$  must be removed from the above described system of equations. Notice that the problem above is over-determined. The minimum-squared error solution for  $\mathbf{r}_S^B$  can be found with the well-known least-squares technique. At each sampling instance,  $\mathbf{r}_S^B$  is calculated and normalized for use with the SVD attitude solution method.

## B. Acceleration Vector from Accelerometer

The acceleration vector information in the body frame was obtained using a MEMS accelerometer. The accelerometer measures two components, the acceleration of the body frame relative to an inertial frame and the acceleration due to gravity. Assuming that the input/output relationship of the accelerometer is linear, the following equation can be formulated:

$$\mathbf{V}_a = K (\dot{\mathbf{r}}_a^B + \mathbf{g}^B) + \mathbf{c} \tag{16}$$

where  $\dot{\mathbf{r}}_a^B$  is the acceleration of the the body frame relative to the inertial frame and  $\mathbf{g}^B$  is the gravitational acceleration vector which are both measured with respect to the body frame. Additionally,  $\mathbf{V}_a$  is a vector of the measured voltages from the accelerometer in the x, y, and z components; K is a matrix of sensitivity coefficients; and  $\mathbf{c}$  is a vector of bias coefficients. The bias coefficients can be determined under a zero-motion

condition as the voltage that is measured on a sensitive axis of the accelerometer that is orthogonal to the gravitational acceleration.

Once the bias coefficients are obtained, one can form the following system of equations and solve for the elements in  $\mathbf{K}$ :

$$\begin{bmatrix} \mathbf{V}_a^{x_g} - \mathbf{c} \\ \mathbf{V}_a^{y_g} - \mathbf{c} \\ \mathbf{V}_a^{z_g} - \mathbf{c} \end{bmatrix} = \begin{bmatrix} 9.81 & 0 & 0 & 0 & 0 & 0 & 0 & 0 & 0 \\ 0 & 0 & 0 & 9.81 & 0 & 0 & 0 & 0 & 0 \\ 0 & 0 & 0 & 0 & 0 & 0 & 9.81 & 0 & 0 \\ 0 & 9.81 & 0 & 0 & 0 & 0 & 0 & 0 & 0 \\ 0 & 0 & 0 & 0 & 9.81 & 0 & 0 & 0 & 0 \\ 0 & 0 & 0 & 0 & 0 & 0 & 0 & 9.81 & 0 \\ 0 & 0 & 9.81 & 0 & 0 & 0 & 0 & 0 & 0 \\ 0 & 0 & 0 & 0 & 0 & 9.81 & 0 & 0 & 0 \\ 0 & 0 & 0 & 0 & 0 & 0 & 0 & 0 & 9.81 \end{bmatrix} \begin{bmatrix} K_{11} \\ K_{12} \\ K_{13} \\ K_{21} \\ K_{22} \\ K_{23} \\ K_{31} \\ K_{32} \\ K_{33} \end{bmatrix} \quad (17)$$

Here,  $\mathbf{V}_a^{x_g}$ ,  $\mathbf{V}_a^{y_g}$ , and  $\mathbf{V}_a^{z_g}$  are the voltages measured on the accelerometer when the x, y, and z components of the body frame are opposite to that of the acceleration vector due to gravity, respectively.

Once both the bias and sensitivity calibration coefficients are determined, one can solve for the acceleration vector. By following the above procedures, the following relationship was obtained:

$$\ddot{\mathbf{r}}_a^B = \begin{bmatrix} 0.0234 & 0.0237 & 0 \\ -0.0151 & 0.0154 & 0 \\ -0.0004 & 0 & -0.0160 \end{bmatrix}^{-1} \left( \mathbf{V}_a - \begin{bmatrix} 1.4171 \\ 1.6419 \\ 1.8154 \end{bmatrix} \right) \quad (18)$$

Note that the orientation of the accelerometer with respect to the payload is arbitrary as the calibration technique proposed here will correct for misalignment. The equation resulting from the calibration procedure was validated with ground tests.

Throughout much of the flight, particularly before balloon-burst, the acceleration of the payload is relatively small. Therefore, the primary component of the measured acceleration is the gravitational vector. Before implementing  $\ddot{\mathbf{r}}_a^B$  into the SVD method to solve for an attitude, it needs to be normalized at each sample instance.

### III. Experimental Results

The experimental data depicted here was from the ANSR (Arizona Near Space Research) flight for the Arizona Space Grant ASCEND (Aerospace Scholarships to Challenge and Educate New Discoverers) Project, held on March 29th, 2014. The payload used for this flight is depicted in Fig. 2. The balloon burst altitude recorded for this flight was approximately 73,794 ft.

To determine the accuracy of and to validate the proposed attitude determination system, the angular velocity information from the rate gyroscope (i.e., experimental data) was compared against the angular velocity information computed from the estimated attitude (i.e., analytical data). Note that both of these vectors are measured with respect to the body frame. The following is a discussion on how to obtain the angular velocity vector from the rate gyroscope in the body frame.

#### A. Angular Velocity Vector From Rate Gyroscope

Obtaining the angular velocity vector consists of a similar process that is described for obtaining the acceleration vector from the accelerometer. The angular velocity information in the body frame was obtained using a MEMS rate gyroscope. The following relationship can be formulated to represent the angular velocity in the body frame:

$$\mathbf{V}_\omega = S\boldsymbol{\omega}^B + \mathbf{b} \quad (19)$$

where  $\mathbf{V}_\omega$  is a vector of the measured voltages from the rate gyroscope in the x, y, and z components;  $\boldsymbol{\omega}^B$  is the angular velocity vector measured in the body frame;  $S$  is a matrix of sensitivity coefficients; and  $\mathbf{b}$  is

a vector of bias coefficients. The bias coefficients are easily found by measuring the voltage during zero-spin conditions. Once the bias voltages have been obtained, the elements of  $S$  are found by solving the following system of equations:

$$\begin{bmatrix} \mathbf{V}_a^{x_{rot}} - \mathbf{b} \\ \mathbf{V}_a^{y_{rot}} - \mathbf{b} \\ \mathbf{V}_a^{z_{rot}} - \mathbf{b} \end{bmatrix} = \begin{bmatrix} \omega_x & 0 & 0 & 0 & 0 & 0 & 0 & 0 & 0 \\ 0 & 0 & 0 & \omega_x & 0 & 0 & 0 & 0 & 0 \\ 0 & 0 & 0 & 0 & 0 & 0 & \omega_x & 0 & 0 \\ 0 & \omega_y & 0 & 0 & 0 & 0 & 0 & 0 & 0 \\ 0 & 0 & 0 & 0 & \omega_y & 0 & 0 & 0 & 0 \\ 0 & 0 & 0 & 0 & 0 & 0 & 0 & \omega_y & 0 \\ 0 & 0 & \omega_z & 0 & 0 & 0 & 0 & 0 & 0 \\ 0 & 0 & 0 & 0 & 0 & \omega_z & 0 & 0 & 0 \\ 0 & 0 & 0 & 0 & 0 & 0 & 0 & 0 & \omega_z \end{bmatrix} \begin{bmatrix} S_{11} \\ S_{12} \\ S_{13} \\ S_{21} \\ S_{22} \\ S_{23} \\ S_{31} \\ S_{32} \\ S_{33} \end{bmatrix} \quad (20)$$

where  $\mathbf{V}_a^{x_{rot}}$ ,  $\mathbf{V}_a^{y_{rot}}$ , and  $\mathbf{V}_a^{z_{rot}}$  are the voltages measured by spinning the payload about the x, y and z components of the body frame at a known constant angular velocity, respectively. A turn-table was utilized to perform this calibration and to measure the constant angular velocities about each of the body axes:  $\omega_x$ ,  $\omega_y$ , and  $\omega_z$ .

Once both the bias and sensitivity calibration coefficients are determined, one can solve for the angular velocity vector. By following the above procedures, the following relationship was obtained:

$$\boldsymbol{\omega}^B = \begin{bmatrix} 0.0032 & 0.0026 & -0.1941 \\ -0.1363 & 0.1327 & 0.0025 \\ 0.1399 & 0.1394 & 0.0056 \end{bmatrix}^{-1} \left( \mathbf{V}_\omega - \begin{bmatrix} 1.4865 \\ 1.4892 \\ 1.4844 \end{bmatrix} \right) \quad (21)$$

Note that the orientation of the rate gyroscope with respect to the payload is arbitrary as the calibration technique proposed here corrects for misalignment. The equation resulting from the calibration procedure was validated with ground tests.

## B. Angular Velocity Vector from Estimated Attitude

The estimated attitude was parameterized in the form of a DCM. The DCM can be differentiated with respect to time, using a finite difference. There is a relationship between the differentiated DCM, the DCM, and a skew-symmetric matrix containing the angular velocity information in the body frame, which can be depicted by the following:

$$\dot{T}_B^A = T_B^A \begin{bmatrix} 0 & -\omega_z^B & \omega_y^B \\ \omega_z^B & 0 & -\omega_x^B \\ -\omega_y^B & \omega_x^B & 0 \end{bmatrix} \quad (22)$$

The relationship above can be easily rearranged to solve for the skew-symmetric matrix after which  $\boldsymbol{\omega}^B$  can be extracted. Thus, accuracy of the DCM can be evaluated, invariant to a particular choice of inertial frame, by comparing the angular velocity vector that is computed from the DCM against the angular velocity vector that was measured by the rate gyroscope.

For this work, a central difference was utilized to time-differentiate the DCM obtained by solving Wahba's problem using the sun sensor data and accelerometer data. The differentiation process introduces noise into the resulting data, thus an ideal low-pass filter was implemented to filter noise from each component of the calculated angular velocity vector. The break frequencies selected for the filter along the x, y and z components were 2.3, 2.0, and 0.8 (rad/s), respectively. The following is the discussion on the results and possible sources of errors.

## C. Results

The angular velocity that was measured from the rate gyroscope (in the body frame) was compared against the angular velocity that was derived from the attitude (in the body frame) to determine the accuracy of the proposed attitude determination system. This comparison, for the entire flight, is depicted in Fig. 5.

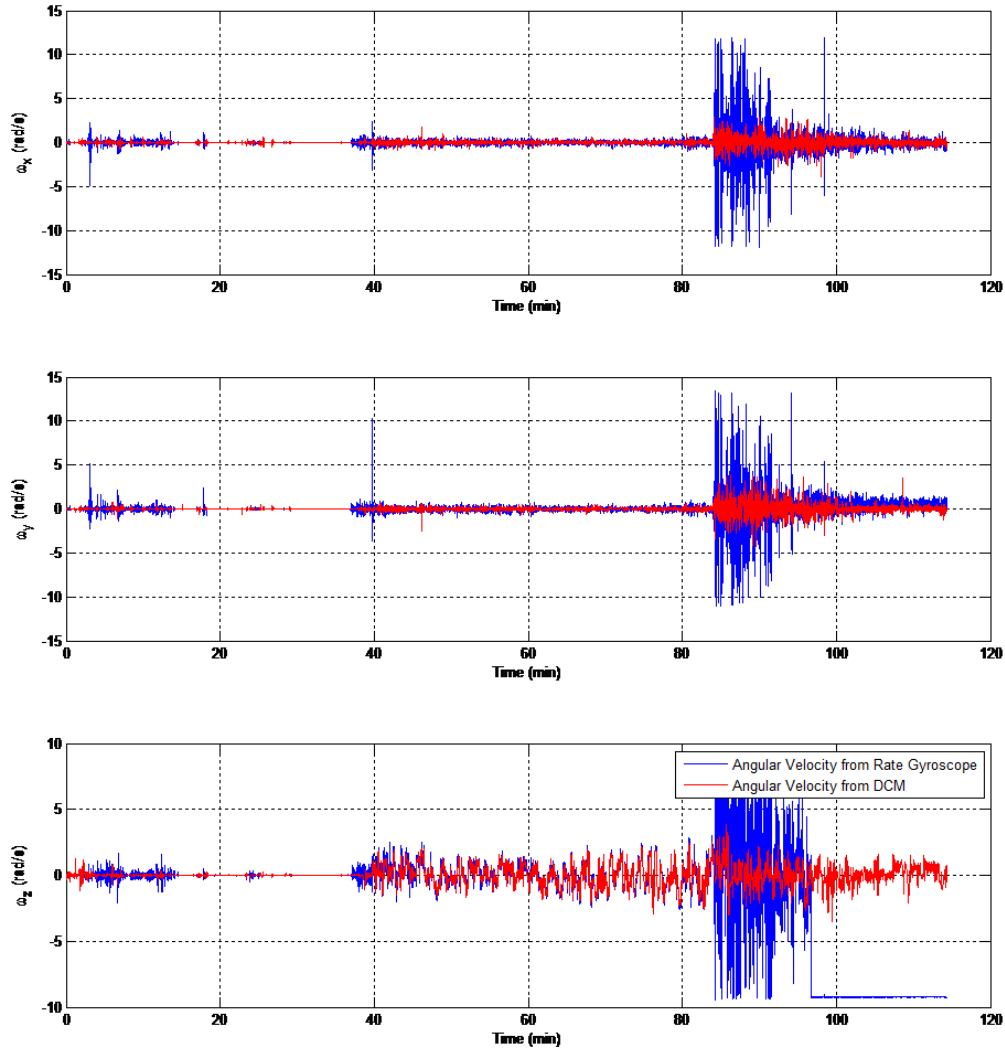


Figure 5. Angular velocity comparison for entire flight.

In Fig. 5, there are four significant time events depicted for the flight. The beginning time stamp of the plot depicts the commencement of data logging. At approximately 40 min, the launch occurs; at approximately 84 min, the balloon bursts; and at approximately 94 min, the payload hits the ground. Therefore, the ascent profile of the flight is depicted between 40 min and 84 min, and the descent profile of the flight is depicted between 84 min and 94 min. Also, depicted in this plot is that during the ascent profile, most of the rotation is felt about the z-axis as the z component has higher relative magnitude compared to that of the x and y components. This is expected due to the geometry of the payload and the nature of the flight itself.

The blue curve in Fig. 5 depicts the angular velocity that was measured using the rate gyroscope, and the red curve depicts the angular velocity that was derived from the computed attitude. This plot portrays that the magnitude for the ascent profile of the flight matches up quite well between the two quantities. However, during the descent, the rate gyroscope data becomes erroneous as it measures collision information. Additionally, since the accelerometer measures not only collisional information but also significantly more acceleration than just the gravitational vector during the descent, it is difficult to determine the accuracy of the angular velocity that was derived from the attitude, during the descent of the flight.

To analyze how well the accuracy of the trend was maintained for the angular velocity that was derived from the attitude, a certain region of the ascent profile was examined closely for all 3 components which is

depicted in Fig. 6.

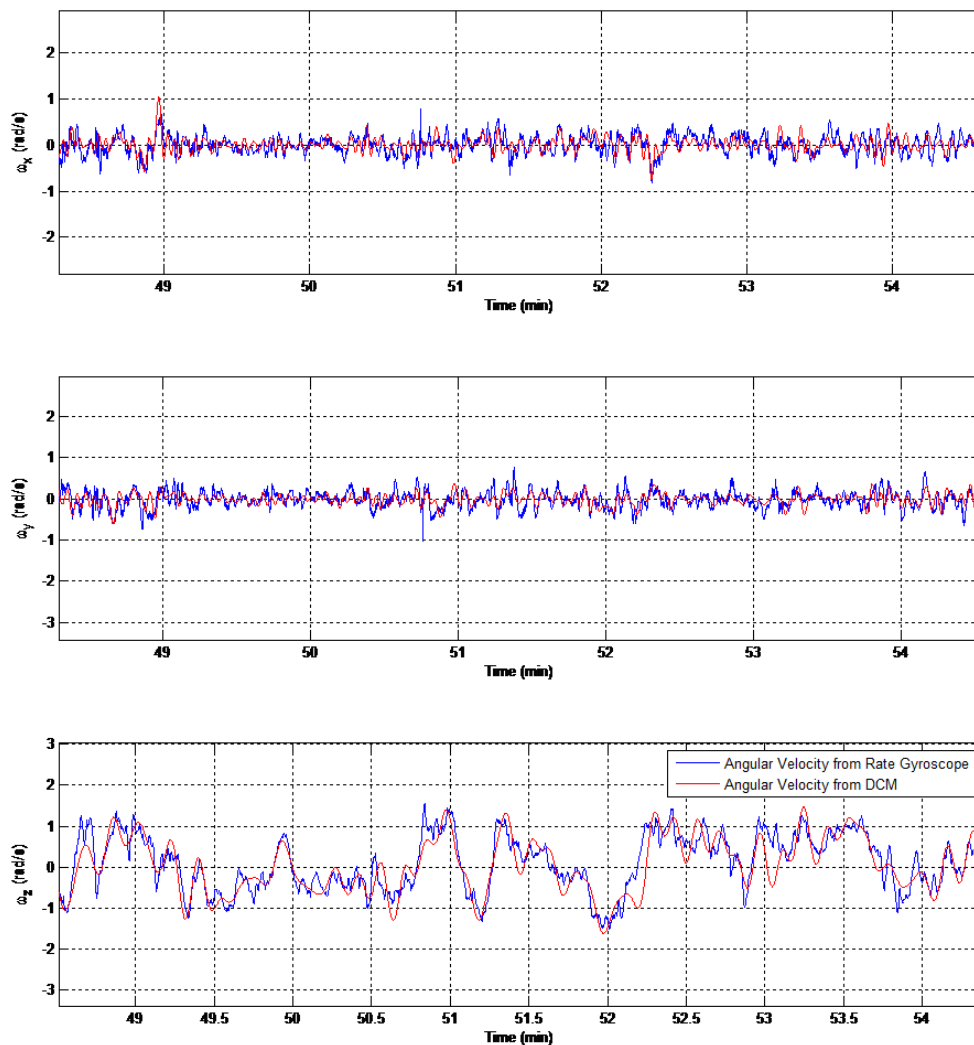


Figure 6. Trend comparison during ascent portion of flight.

Both of the angular velocity vectors are measured independently of each other as the attitude was computed using the acceleration and sunlight vectors, while the angular velocity was measured from an independent sensor. As depicted by Fig. 6, the z component of the angular velocity vector derived from the attitude matches up quite well with the z component of the angular velocity vector measured using the rate gyroscope. This demonstrates the accuracy of the attitude determination system proposed in this paper. The x and y components, however, seem to have a much lower signal-to-noise ratio as relatively less rotation occurred about these two axes.

#### IV. Conclusion

This paper discussed an attitude determination system for high-altitude balloon flights using low-cost sensors. There is high interest in the field and its applications such as Earth-related observations. The attitude determination system proposed in the paper utilizes Markley’s SVD solution to Wahba’s problem. Two independent sets of vector quantities were utilized in the SVD solution: the sunlight vector and the acceleration vector. To obtain the body frame sunlight vector measurements, a sun sensor consisting of 23 solar cells was used. To obtain the body frame gravitational vector measurements, a 3-axis accelerometer

was used. The final attitude was parameterized in a DCM for each sample instance.

The attitude computed, at each sample instance, was differentiated and filtered to extract the angular velocity information in the body frame. This result was compared against the angular velocity which was experimentally obtained in the body frame using a 3-axis rate gyroscope. The results portray that both the magnitude and trend between the angular velocity measured using the rate gyroscope and the angular velocity computed from the estimated attitude match up quite well for the ascent profile of the flight. This demonstrated the accuracy of the attitude determination system proposed here for the application of high-altitude balloon flights.

Possible recommendations for future research include obtaining more than two sets of independent vector quantities, perhaps by introducing the magnetic field vector. Additionally, since an accelerometer will measure not only the gravitational acceleration, but all accelerations (including collisions), utilizing only the magnetic field vector and the sunlight vector may result in a more accurate attitude determination system. Also, validating the accuracy of the estimated attitude by utilizing the angular velocity vector requires the DCM to be differentiated. However, this introduces noise and phase shifts. It would be ideal to measure the attitude of the payload using some other method such as image/video digital signal processing to obtain roll, pitch, and yaw; so that the attitude estimation algorithm can be directly validated against a measured attitude.

## Acknowledgments

The authors would like to thank the Embry-Riddle Aeronautical University College of Engineering and the Arizona Space Grant Consortium for providing funding for this project, Jack Crabtree and the Arizona Near Space Research non-profit for assisting with the launch, PowerFilm Solar Inc. for donating the 26 solar cells that were utilized to carry out this research, and the following students who made contributions towards the construction and launch of the experimental gondola: Benjamin Anderson, Dallas Hodge, Austin Leonard, Patrick Deskin, Loren Williams, John Cybulski, and Brigette Cochran.

## References

- <sup>1</sup><http://www.google.com/loon/>, "Google Loon," 2014.
- <sup>2</sup>Whitmore, S. A., Fife, M., and Brashear, L., *Development of a closed-loop strap down attitude system for an ultrahigh altitude flight experiment*, Vol. 4775, National Aeronautics and Space Administration, Office of Management, Scientific and Technical Information Program, 1997.
- <sup>3</sup>Quine, B. M., Strong, K., Wiacek, A., Wunch, D., Anstey, J. A., and Drummond, J. R., "Scanning the Earth's limb from a high-altitude balloon: The development and flight of a new balloon-based pointing system," *Journal of Atmospheric and Oceanic Technology*, Vol. 19, No. 5, 2002, pp. 618–632.
- <sup>4</sup>Schneeberger, T. J. and Barker, K. W., "High-altitude balloon experiment: a testbed for acquisition, tracking, and pointing technologies," *Optical Engineering and Photonics in Aerospace Sensing*, International Society for Optics and Photonics, 1993, pp. 2–15.
- <sup>5</sup>Zhu, R., Sun, D., Zhou, Z., and Wang, D., "A linear fusion algorithm for attitude determination using low cost MEMS-based sensors," *Measurement*, Vol. 40, No. 3, 2007, pp. 322–328.
- <sup>6</sup>Lefferts, E. J., Markley, F. L., and Shuster, M. D., "Kalman filtering for spacecraft attitude estimation," *Journal of Guidance, Control, and Dynamics*, Vol. 5, No. 5, 1982, pp. 417–429.
- <sup>7</sup>Gebre-Egziabher, D., Elkaim, G. H., Powell, J., and Parkinson, B. W., "A gyro-free quaternion-based attitude determination system suitable for implementation using low cost sensors," *Position Location and Navigation Symposium, IEEE 2000*, IEEE, 2000, pp. 185–192.
- <sup>8</sup>Li, Y., Dempster, A., Li, B., Wang, J., and Rizos, C., "A low-cost attitude heading reference system by combination of GPS and magnetometers and MEMS inertial sensors for mobile applications," *Positioning*, Vol. 1, 2006, pp. 0.
- <sup>9</sup>Wahba, G., "A least squares estimate of satellite attitude," *SIAM review*, Vol. 7, No. 3, 1965, pp. 409–409.
- <sup>10</sup>Markley, F. L., "Attitude determination using vector observations and the singular value decomposition," *The Journal of the Astronautical Sciences*, Vol. 36, No. 3, 1988, pp. 245–258.
- <sup>11</sup>Keat, J. E., "ANALYSIS OF LEAST-SQUARES ATTITUDE DETERMINATION ROUTINE DOAOP," 1977.
- <sup>12</sup>Shuster, M. D., "Approximate algorithms for fast optimal attitude computation," *AIAA Guidance and Control Conference*, AIAA New York, NY, 1978, pp. 88–95.
- <sup>13</sup>Markley, F. L. and Mortari, D., "Quaternion attitude estimation using vector observations," *Journal of the Astronautical Sciences*, Vol. 48, No. 2, 2000, pp. 359–380.
- <sup>14</sup><http://www.esrl.noaa.gov/gmd/grad/solcalc/azel.html>, "NOAA," 2014.